ELSEVIER

Thin Solid Films 303 (1997) 66–75

thin solid films

Si-containing crystalline carbon nitride derived from microwave plasma-enhanced chemical vapor deposition

L.C. Chen [a,*], D.M. Bhusari [b], C.Y. Yang [b], K.H. Chen [a,b], T.J. Chuang [b], M.C. Lin [c], C.K. Chen [a], Y.F. Huang [d]

[a] *Center for Condensed Matter Sciences, National Taiwan University, Taipei, Taiwan*
[b] *Institute of Atomic and Molecular Sciences, Academia Sinica, Taipei, Taiwan*
[c] *Department of Chemistry, Emory University, Atlanta, GA, USA*
[d] *Department of Physics, Fu-Jen University, Taipei, Taiwan*

Received 2 October 1996; accepted 16 January 1997

Abstract

Carbon nitride thin films have been grown by the microwave plasma-enhanced chemical vapor deposition (MW-PECVD) technique. Gas mixtures containing CH_4, H_2 and NH_3 at various ratios were tested as precursors, and Si (100) wafers were used as substrates. X-ray photoelectron spectroscopy (XPS), Auger electron spectroscopy (AES), electron microscopy (both SEM and TEM), and Raman spectroscopy have been employed to characterize the resultant films. The phase contents in the films were found to be strongly dependent on the substrate temperature. The incorporation of significant amounts of Si into the film was observed when the substrate temperature exceeded 1000 °C. However, the presence of Si along with a high substrate temperature also promotes the formation of large crystallites. XPS analyses of C(1s) and N(1s) core levels suggest a multiple bonding structure between carbon and nitrogen atoms. Microscopic investigations of the films reveal the coexistence of large grain (> 10 μm) and fine grain (< 1 μm) crystals. Preliminary structural studies suggest the presence of a crystalline carbon nitride compound corresponding to a hypothetical α-C_3N_4 phase (isomorphic to α-Si_3N_4), which may also be a stable hard material. Furthermore, we propose that some of the Si has been incorporated as a substitutional element for the C site in the new phase. The Raman spectra exhibit many sharp lines, of which the most distinct ones mimic those of the α-Si_3N_4 structure. © 1997 Elsevier Science S.A.

Keywords: Chemical vapour deposition (CVD); Nitrides; Transmission electron microscopy (TEM); X-ray photoelectron spectroscopy (XPS)

1. Introduction

Recently, considerable research effort has been directed toward the growth of carbon nitride films. An early unpublished patent disclosure and theoretical studies suggest that a tetrahedral compound of carbon and nitrogen, isomorphic in structure to β-Si_3N_4, might have a bulk modulus comparable to that of diamond [1–3]. So far, there have been several reports on the deposition of carbon nitride and its hydrogenated variant by various PVD as well as CVD processes [4–12]. However, most of these techniques did not succeed in synthesizing crystalline C_3N_4 phase. While some crystalline carbon nitride solid has been obtained by pulsed laser ablation [10], rf diode sputtering [11], and dual ion beam sputtering [12], the fit of their diffraction data to that of the predicted β-C_3N_4 structure was only partially successful. In fact, more recent theoretical studies have also investigated the stability and properties of C_3N_4 compounds that have structures distinct from the β-C_3N_4 structure. For instance, Liu and Wentzcovitch suggested that defective zincblende and rhombohedral graphite-like structures should have stabilities comparable to or greater than that of β-C_3N_4 [13]. Guo and Goddard [14] further suggested that the reported transmission electron diffraction (TED) data of carbon nitride films obtained by Yu et al. [11] are better indexed for α-C_3N_4, which is also more stable than β-C_3N_4. Nonetheless, the fit of the peak positions and their intensities between the newly hypothesized α-C_3N_4 structure and the experimental data is by no means perfect yet.

Besides the fact that the crystal structure of C_3N_4 is not uniquely determined, there is also no reason to assume a

* Corresponding author. Tel: +886 2 366 8228; fax: +886 2 362 0200; e-mail: chenlc@ccms.ntu.edu.tw.

PII S0040-6090(97)00041-2

unique stoichiometry for the carbon nitride compound. Experimentally, all the reported nitrogen-to-carbon ratios are much lower than that in the stoichiometric C_3N_4. Significantly, Zhang et al. reported that the dominant phase in their carbon nitride film prepared by pulsed laser ablation was C_2N [15]. Because of these uncertain situations, many metastable phases must be carefully considered in experimental studies of this new class of materials.

Stimulated by the successful implementation of plasma-enhanced chemical vapor deposition to produce high-quality diamond and silicon nitride, we have adopted the method to synthesize carbon nitride solid. A mixture of CH_4, NH_3 and H_2 was used as the source gas. Detailed chemical information, including the composition and bonding states in the resultant film, was obtained by X-ray photoelectron spectroscopy. In addition, X-ray diffraction, transmission electron microscopy as well as Raman spectroscopy were used to further investigate the film structure. Usually, crystal growth is promoted at elevated temperatures due to the enhanced mobility of surface atoms. However, Cuomo et al. reported that the deposition of CN_x goes to zero at substrate temperatures above 627 °C [16]. We believe that the high substrate temperature strategy would still be applicable if the crystal formed is stable at the temperature under experiment. Recently, Niu et al. reported that the carbon nitride film formed by pulsed laser ablation is stable up to 800 °C, which is the maximum temperature they tested [10]. In order to explore the possibility of improving the crystallinity of carbon nitride, we have performed the CVD process at high substrate temperatures.

2. Experimental

The carbon nitride films were prepared by microwave plasma-enhanced CVD (MW-PECVD) method in an AsTex 5 kW microwave reactor. The films were deposited on Si (100) substrates after standard HF acid deoxidization and distilled water cleaning. A mixture of semiconductor grade NH_3, CH_4 and H_2 gases in various proportions was used as the source gas. No separate substrate heating was used. The substrate temperature varied depending primarily on the microwave power, the composition and flow rate of the source gas. An optical pyrometer was used to measure the substrate temperature. Typical experimental conditions are listed in Table 1.

A Renishaw system 2000 micro-Raman spectrometer was used to record the Raman spectra. A 25 mW HeNe laser operating at 632 nm was used as an excitation source. The line shift was calibrated by comparing the spectrum with that of natural diamond and Si. With a 5 micron exit slit, the spectral resolution was better than 1 cm^{-1}. The chemical state of the film was determined by X-ray photoelectron spectroscopy (XPS) using a VG Microtech MT-500 ESCA system. Mg Kα radiation of 1253.6 eV was used as the source with a linewidth of 0.7 eV. The typical analyzer pass energy was 20 eV. Curve-fitting software (ESCA-Tools) provided by Surface Interface was used to analyze the XPS data. The experimental uncertainty in the determination of the binding energy is about ±0.4 eV. Depth profiling with XPS and Auger electron spectroscopy (AES) were performed by Ar^+ ion bombardment of the sample. A Perkin Elmer scanning Auger nanoprobe system (SAN 760) was used for the AES study. It should be noted that the X-ray probe size for XPS study is inherently larger than the individual crystal size. In contrast, the AES system is capable of acquiring the depth profile data from area as small as 500 Å, thus allowing us to investigate the variations in composition from crystal to crystal in the same film. A Rigaku D/MAX-3C X-ray diffractometer was used to study the structure of the deposited film. The Cu Kα line at 1.54 Å was used as the source for diffraction. Transmission electron microscopy (TEM) investigations of the film were performed on a Hitachi H-7100 microscope at an operating voltage of 75 kV. The specimens were prepared by scraping and grinding the film, suspending the resulting fragments in methyl alcohol, and finally depositing the suspension onto the Cu grid.

Table 1
Typical deposition conditions for microwave plasma-enhanced CVD

Source	$H_2+CH_4+NH_4$
$[H_2]$:$[CH_4]$:$[NH_3]$ (sccm)	120:20:60
Total flow rate (sccm)	200
Microwave power (W)	2500–3500
Total pressure (Torr)	80
Substrate temperature (°C)	1000–1200

3. Results and discussion

3.1. General characteristics

Process gas mixtures containing CH_4, H_2 and NH_3 at various ratios were used in the experiments. If CH_4 was too high, diamond-like carbon deposition was observed. Well-faceted crystallites were deposited for CH_4:NH_3 ratios between 1:3 and 1:8 and substrate temperatures of 1250–1000 °C. Within these ranges of CH_4:NH_3 ratio and substrate temperature, but otherwise similar microwave powers, total flow rates, and total pressures, as listed in Table 1, all the resultant films consisted of predominantly rod-shaped crystals.

A typical SEM micrograph of our MW-PECVD sample shows large crystallites of dimensions of the order of tens of microns (Fig. 1(a)). The film appears transparent and the crystals are randomly oriented on the substrate. Many rod-shaped crystals exhibit hexagonal cross sections (Fig. 1(b)). The growth rates of these crystals are apparently larger along their length than along their width. The typical

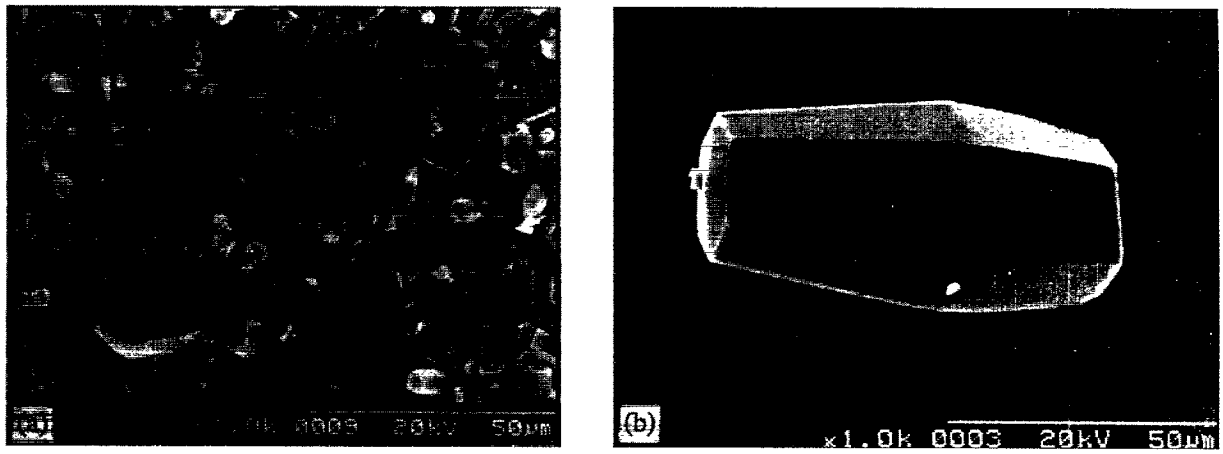

Fig. 1. (a) Typical SEM micrograph of silicon-containing carbon nitride film. (b) Representative rod-shaped crystal exhibiting a six-sided cross section.

rod length to width ratio is about 5–10. Under our experimental conditions, deposition rates were of the order of 1 $\mu m\ h^{-1}$.

3.2. Chemical composition and bonding

A typical wide-scan XPS spectrum of an as-deposited film is presented in Fig. 2, which shows the presence of Si, C, N and O in the material. The oxygen peak at 533 eV, however, almost disappeared after sputtering with Ar^+ ions, indicating that oxygen is present mostly on the surface, while only a trace amount of oxygen is incorporated in the crystals. The Si, C and N peaks, on the other hand, remained constant throughout the depth profiling, suggesting that these peaks are derived from the deposition. High-resolution XPS scans of Si(2p), C(1s) and N(1s) peaks for two samples prepared using gas mixtures containing $[CH_4]$:$[NH_3]$ ratios of 1:3 and 1:6 but under otherwise identical conditions, are presented in Figs. 3–5, respectively. These spectra reveal that all the peaks consist of more than one Gaussian peak, indicating multiple bonding structures between the constituent atoms Si, C and N. The Si(2p) photoelectron peaks could be resolved into three peaks centered at 99.2–99.9, 101.6–102.7 and 103.5–104.6 eV, and belong to Si(2p)–Si, Si(2p)–N and Si(2p)–O bonding, respectively. The Si–Si peak is believed to originate from the Si substrate surface uncovered by the crystals and is not derived from the crystals. Notably, there is no major separate peak that matches the Si(2p)–C binding energy of 100.3 eV, thus suggesting the absence of Si–C bonds in the material. The C(1s) photoelectron peak consists of two components centered at 284.8–285.7 and 287.2–288.4 eV, whereas the N(1s) peak also consists of two components centered at 397.5–398.5 and 399.5–400.6 eV. Although the assignment of these C(1s) and N(1s) photoelectron peaks to some specific bonding structures is not as straightforward as those of Si(2p) peaks, the shift in the C(1s) binding energy to a higher value compared to that of the C–C bond in diamond or graphite (284.5 eV) confirms the bonding of carbon with more electronegative nitrogen. Consistent with the results for the Si(2p) peaks where no major Si(2p)–C

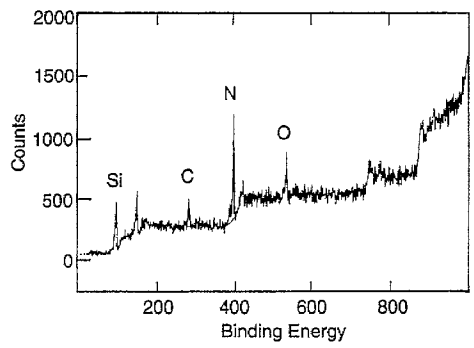

Fig. 2. Typical wide-scan XPS spectrum of silicon-containing carbon nitride film prepared under the process conditions listed in Table 1.

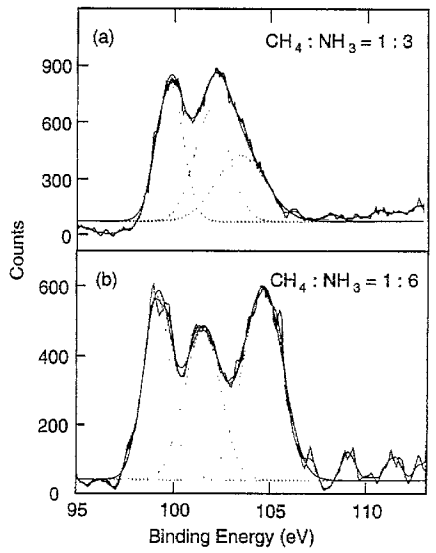

Fig. 3. XPS Si(2p) spectra of Si–C–N films prepared (a) under the process conditions listed in Table 1, or those for sample A in Table 3; and (b) under process conditions similar to those in (a) except that the $[H_2]$:$[CH_4]$:$[NH_3]$ was 120:10:60, or sample E in Table 3.

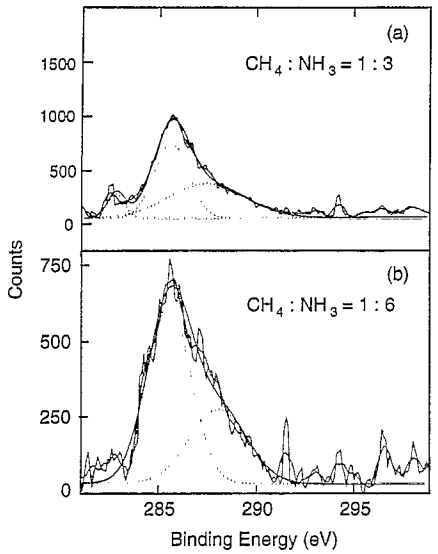

Fig. 4. Corresponding XPS C(1s) spectra of Si–C–N films prepared under two different sets of conditions as stated in Fig. 3.

bonding is observed, the C(1s) peaks also show little C(1s)–Si bonding in the vicinity of 282.8 eV [17]. As can be seen from Fig. 4(b), it is arguable whether C(1s)–Si bonding is present at all in the film prepared using a $[CH_4]$:$[NH_3]$ ratio of 1:6, although a trace amount of C(1s)–Si bonding is visible in the film prepared using a $[CH_4]$:$[NH_3]$ ratio of 1:3 (Fig. 4a). However, the area of this peak is an order of magnitude smaller than that of the main peak. Thus the presence of Si–C bonds in these crystals is believed to be negligible.

For comparison, Table 2 summarizes the average values for the C(1s) and N(1s) binding energies pertaining to the carbon–nitrogen bonding configuration obtained in the present work, together with some values reported in the literature [8,10,18–23]. Most of the reported values for C(1s) and N(1s) peaks in the CN_x films vary in the ranges 284–285 and 398–399 eV, respectively.

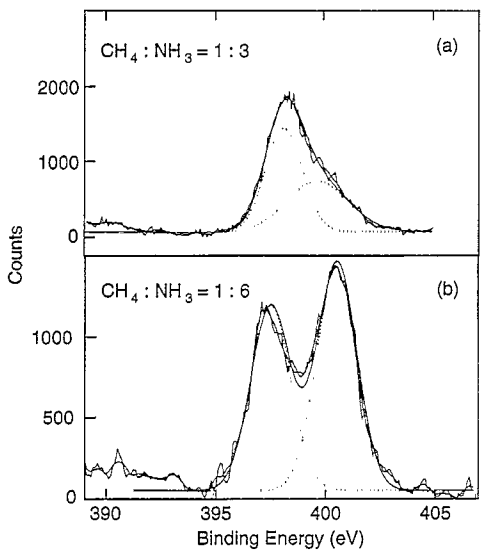

Fig. 5. Corresponding XPS N(1s) spectra of Si–C–N films prepared under two different set of conditions as stated in Fig. 3.

Table 2
Average XPS peak positions (in eV) for five samples prepared under four different process conditions (given in Table 3). Literature values for XPS peak positions are also listed for comparison

Reference	Deposition method	C(1s)	N(1s)
Present work	Microwave CVD	285.5, 287.7	398.1, 400.2
[8]	Ion and vapor deposition	284, 285.8	398.5
[10]	Pulsed laser abaltion + atomic N	284.6	399.1
[18]	Rf reactive sputtering	285	399.2
[19]	ECR plasma + vapor deposition	284.8	398.6
[20]	NH_3 ion-beam-assisted deposition	284.5–284.8	398.2–398.9
[21]	Ion and vapor deposition	286.3	398.4
[22]	Various techniques	286.1, 287.7	398.5, 400
[23]	Nitrogen implantation	–	398.4, 399.6

Marton et al. [22] compared the C and N binding energies in the CN_x films deposited by three different techniques with those in chemical compounds containing C–N and C=N bonds. They suggested a binding energy of 287.7 ± 0.2 eV for the sp^3 bonded C(1s)–N structure and 286.1 ± 0.2 eV for the sp^2 bonded C(1s)–N structure. The corresponding N(1s)–C binding energies were suggested to be 398.5 ± 0.2 and 400 ± 0.3 eV, respectively. It is likely that the two C(1s) peak positions at 285.6–285.7 and 287.4–288.4 eV observed in our films reflect the presence of these two different bonding states between carbon and nitrogen. However, if this is the case, one should also observe two corresponding bonding structures in the N(1s)–C peaks. Although we do observe two peaks in the N(1s) spectrum, the lower energy peak (397.6–398.4 eV) has to be assigned to N(1s)–Si bonding since the Si(2p) spectrum contains a very prominent Si–N peak. In pure Si_3N_4, the energy of this N(1s)–Si bonding is 397.5 eV [24]. This peak is, however, likely to shift to higher energy in the present ternary crystals if Si–N–C type bonding is present, due to the higher electronegativity of C than Si. Thus, the assignment of the lower-energy peak in the N(1s) spectrum to N–Si bonding leaves us with only one peak corresponding to the N–C bonding, which is inconsistent with the C(1s) XPS. This inconsistency, however, can not be addressed with the present level of our understanding of the crystal structure and various C–N bonding environments. Meanwhile, Hoffman et al. observed three types of N(1s) bonding configurations: the first one at 398.4 eV was attributed to the cyanide-type groups (–C≡N); a second one at 399.6 eV was an almost unpolarized carbon nitrogen bond (–N <); and the third one at 401.5 eV was associated with a mixture of different –N=N– and > N–N < fragments as well as –N=O bonds [23]. The binding energies of their first and second

states are also shown in Table 2 for comparison. The second state is believed to be characteristic of the C_3N_4 phase.

This tentative assignment of the Si, C and N peaks allows us to make a further evaluation of the film composition. The chemical compositions of five samples prepared under four different $[H_2]$:$[CH_4]$:$[NH_3]$ ratios are compared in Table 3. The [Si]/[N] atomic ratio is calculated from the peak area ratio of the Si(2p)–N to N(1s)–Si signals corrected by their known sensitivity factors (i.e. photoionization cross sections) [25]. The uncertainty in the calculation of the atomic ratios from the integrated XPS intensity and the sensitivity factors is estimated to be $\pm 15\%$. Likewise, the [C]/[N] atomic ratio is calculated from the corresponding ratio of the C(1s)–N to N(1s)–C signals. The average film composition for a Si–C–N film can also be estimated from the sensitivity-factor-corrected [Si]:[C]:[N]. Certainly, the Si(2p)–Si and Si(2p)–O peaks are incidental and are thus excluded from the computation. One should keep in mind that the film may contain multiple phases; therefore, the average film composition should be considered as a reference value, which may not have any physical significance.

Notably, both the [Si]/[N] and [C]/[N] ratios for all of our films are significantly higher than the expected values for Si_3N_4 or C_3N_4 stoichiometry. It may be mentioned here that the typical [Si]/[N] ratio in the silicon nitride films derived from SiH_4–NH_3–N_2 plasma-enhanced CVD also lies between 0.8 and 1.0, which is considerably higher than the theoretical value of 0.75 [26]. This departure from stoichiometric Si_3N_4 composition is attributed to the hydrogenation of the structure. Similar effects may have taken place in our process or there could also be several N vacancy sites. If the film consisted primarily of a single phase represented by the formula $Si_xC_yN_z$, a plausible structure could be that of a Si_3N_4 solid with many of the Si sites being substituted by C. Under such circumstances, the composition ratio of [Si + C]/[N] is a better indicator of the stoichiometry of the film. The [Si + C]/[N] ratios are also shown in Table 3.

The XPS results merely give the gross chemical composition over a large area in which crystal-to-crystal inhomogeneities can not be ruled out. In a separate study, scanning AES with depth profiling and with a probe size of the order of 1 μm was employed to determine the chemical composition of individual crystals. A typical Auger spectrum is shown in Fig. 6(a). Consistent with our XPS results, silicon, carbon, nitrogen and oxygen peaks are observed. The corresponding depth profile is shown in Fig. 6(b), where the atomic concentration of each constituent element is shown. For this particular crystal, except near the surface, [N] varies between 40 and 50 at%, [C] between 40 and 50 at%, [Si] between 5 and 10 at%, and [O] at about 2 at%. For the crystals deposited on the same substrate, we do indeed observe considerable variations in the chemical composition, while the crystal morphology remains unaltered. A more detailed description of our Auger studies is presented elsewhere [27].

Table 3
Estimates of the atomic ratios of [C]/[N], [Si]/[N], [Si + C]/[N], and the average film compositions for five samples prepared under four different process conditions

Sample	$[H_2]$:$[CH_4]$:$[NH_3]$	[Si]/[N]	[C]/[N]	[Si+C]/[N]	[Si]:[C]:[N] (%)
A	120:20:60	0.95	2.34	1.7	20:43:37
B	120:20:60	1.05	2.36	1.63	22:40:38
C	75:15:60	1.45	1.08	1.17	18:36:46
D	120:10:50	1.82	0.81	1.02	18:32:50
E	120:10:60	0.80	1.43	1.17	17:37:46

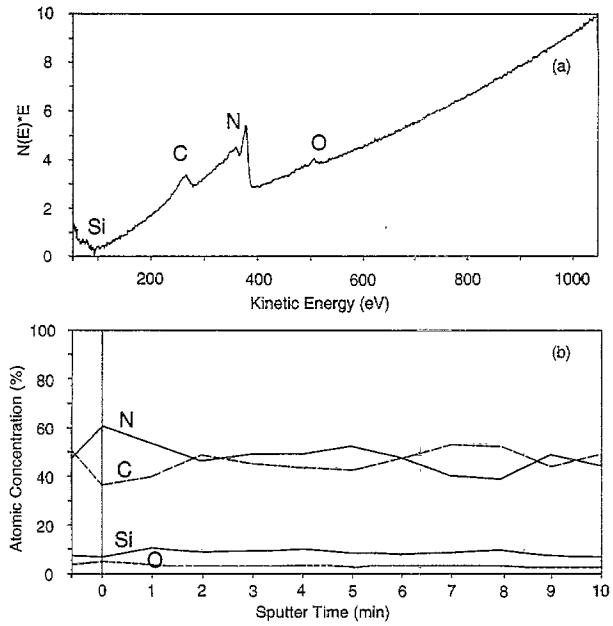

Fig. 6. (a) Typical Auger electron spectrum of our Si–C–N crystal, and (b) the corresponding scanning Auger depth profile of this particular crystal.

3.3. Microstructure

The X-ray diffraction (XRD) spectra of polycrystalline SiCN film (not shown here) display many sharp lines and no broad humps, suggesting the absence of an amorphous phase in the crystalline films. The presence of large numbers of sharp diffraction lines in these spectra further suggest either a crystal structure with low symmetry or the coexistence of mixed phases. The d values (i.e. interplanar spacings), as obtained from the XRD spectra, do not match completely with those of either α- or β-phases of Si_3N_4 [28] or of C_3N_4 [29]. This is obvious since the present ternary alloy would have different lattice spacings even if it retains the same short-range and long-range orders of either the α- or β-phases. One can nevertheless assume a

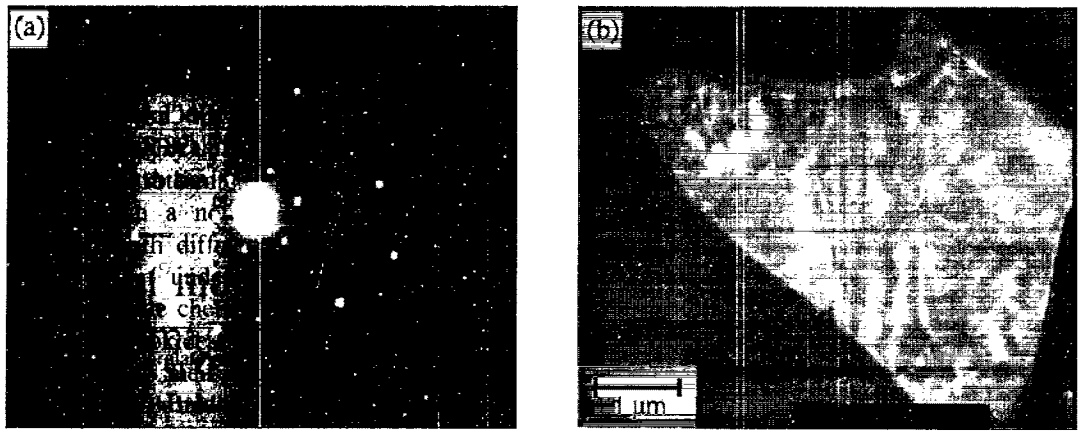

Fig. 7. (a) Transmission electron diffraction pattern of the Si–C–N crystal with hexagonal symmetry. (b) The corresponding dark field image of this crystal.

certain stoichiometry and crystal structure for this material and calculate the corresponding lattice spacings and consequently index the observed diffraction peaks accordingly. But the possibility of the presence of more than one phase in the polycrystalline film does not guarantee that the results thus obtained would be unambiguous. Notably, recent theoretical studies have shown that as many as four different phases of carbon nitride can exist as stable compounds only for the C_3N_4 stoichiometry [13]. Moreover, there is also no reason to believe that C_3N_4 would be the only stable stoichiometry. In fact, recent experimental results have shown that C_2N is a more stable phase than C_3N_4 [15]. Clearly, several phases can be present in the film. In addition to this difficulty, variations in the chemical compositions of individual crystals in the present polycrystalline films, as observed by scanning Auger studies [27], further complicate the analysis of the diffraction spectra. Thus, unambiguous identification of the structure of the present SiCN crystals has not been possible by X-ray diffraction studies.

Transmission electron microscopy (TEM) was then employed to investigate the structure of this new crystalline material. Since this technique probes the structure of an individual crystal, as opposed to XRD which is a bulk technique, these studies were expected to reveal whether multiple phases are present. These investigations indeed revealed the presence of two different microstructures in the film, one giving a single-crystal diffraction pattern, and the other giving a powder diffraction pattern. A detailed analysis of the latter has been published elsewhere [30]. The volume fraction of the specimen that gives a powder diffraction pattern is, however, less than 10%. Since the samples for these studies were prepared by scrapping and grinding the film, the information pertaining to the relative positions of these specimens in the film was lost. However, we believe that the fine-grained polycrystalline material lies only at the interface since the SEM micrographs are overwhelmed by large grain crystals. Typical transmission electron diffraction patterns obtained from one of the large grain crystals are presented in Figs. 7 and 8. As

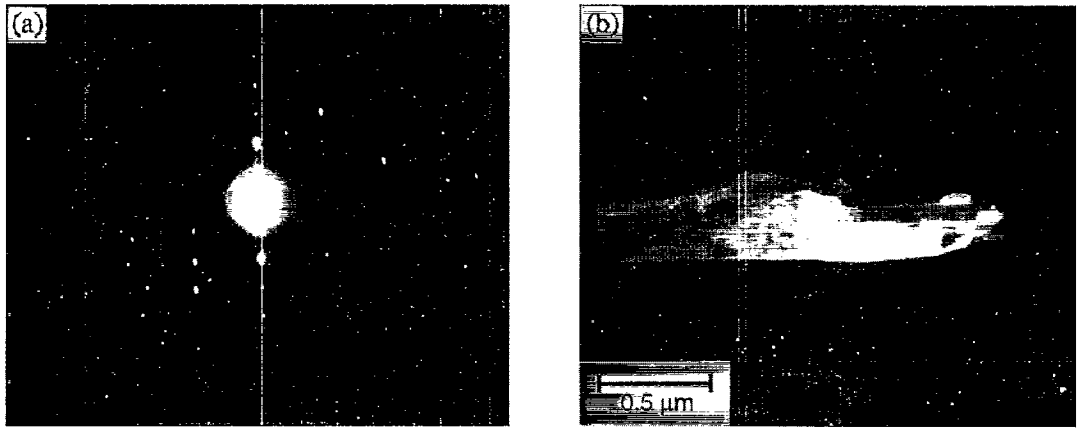

Fig. 8. (a) Transmission electron diffraction pattern of the Si–C–N crystal with twofold symmetry. (b) The corresponding dark field image of this rod-shaped crystal.

expected, the lattice spacings obtained from these diffraction patterns do not match completely with those of either α- or β-phases of Si_3N_4 or C_3N_4 [28,29]. However, since the electron diffraction patterns for these crystals suggest a hexagonal structure, the lattice parameters a and c (as conventionally defined for hexagonal structures) can be calculated. Such a hexagonal structure is consistent with the morphology observed from the SEM micrographs. Preliminary estimates of the magnitudes of a and c are 5.4 and 6.7 Å, respectively. Consistent with the observed variations in the chemical compositions of individual crystals [27], a variation of $\pm 10\%$ in the values of these parameters are observed from crystal to crystal. The fact that the lattice parameter c is much larger than a suggests that these crystals possess a hexagonal structure with a large number of atoms per unit cell. It may be noted here that the α-phase of Si_3N_4 contains a larger number of atoms per unit cell than the β-phase. The unit cell volumes of $Si_xC_yN_z$ crystals, as estimated from the above diffraction data, are between those of α-Si_3N_4 and α-C_3N_4. The possibility that the present crystals have β-phase can be ruled out here since the β-phase would have a much smaller c parameter value. This is because of the fact that the number of atoms per unit cell in the α-phase is twice that in the β-phase, and the β-structure can be described as a stacking of planes ABAB..., whereas the α-structure can be described as a stacking of planes ABCDABCD.... Thus, the magnitude of the lattice parameter c for the α-phase would be almost twice that for the β-phase. The TEM results therefore suggest that the present SiCN crystal may have a structure close to that of α-Si_3N_4.

The scanning Auger studies have confirmed that any of the large crystals are neither "pure" Si_3N_4 nor "pure" C_3N_4 [27]. Hence, the crystals are better described as a $Si_xC_yN_z$ phase, with varying x, y and z. Alternatively, one could also describe the crystal structure as being either that of α-$[Si(C)]_3N_4$ or that of α-$[C(Si)]_3N_4$. The α-$[Si(C)]_3N_4$ phase denotes a solid solution of α-Si_3N_4 structure with some solubility of C, whereas the α-$[C(Si)]_3N_4$ phase denotes a solid solution of α-C_3N_4 structure with some solubility of Si. The fact that the XPS signals for the Si–C bonding states are negligible suggests that Si substitutes only for the C sites, and vice versa. Therefore, C and Si are always bridged by nitrogen in all these crystals. Considering the substitutional nature of the C and Si atoms in these crystals, we name this crystalline material as $(C; Si)_xN_y$.

3.4. Raman study

Besides the diffraction studies, the samples were also analyzed by Raman spectroscopy. Fig. 9 shows a typical Raman spectrum obtained from sample C. Many strong and sharp lines are observed, characteristic of crystals. Some variations in the line positions and relative intensities are observed from crystal to crystal. Notably, there are also two broad Raman bands at 1340 and 1600 cm^{-1}.

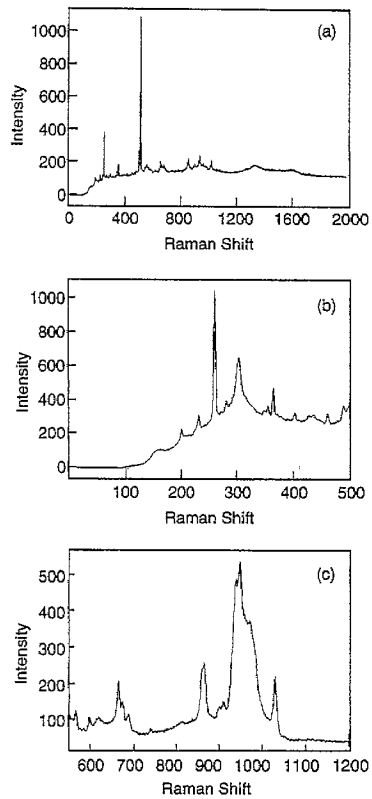

Fig. 9. (a) Typical Raman spectrum for our sample. The lines observed at 531 and 940 cm^{-1} are due to Si. (b) Raman spectrum in the range 0–500 cm^{-1} from the same sample as shown in (a) but in a different region. (c) The corresponding Raman spectrum in the range 550–1200 cm^{-1} of the sample shown in (b).

Similar to the diffraction technique, the Raman spectrum depends strongly on the specific crystallographic symmetry of the sample. By means of group theory analysis, Wada et al. predicted 40 and 11 Raman modes for α- and β-Si_3N_4, respectively [31]. Apparently, the more complex spectrum for α-structure is due to the lower symmetry of the crystal. The experimental observations of Wada et al. for β-Si_3N_4 were in excellent agreement with the theoretical predictions, while α-Si_3N_4 sample exhibited fewer peaks than predicted due to its somewhat poorer optical quality. Nevertheless, up to 30 Raman modes for the α-Si_3N_4 were still observed [31]. In contrast, the Raman spectra of amorphous Si_3N_4 displays only two rather broad peaks. Assuming a topographic analogy between the C_3N_4 and Si_3N_4, one would expect a rather more complex Raman spectrum for α-C_3N_4 than for β-C_3N_4. The many sharp lines observed in the present crystals therefore indicate that these crystals are likely to have lower symmetry, which is consistent with the TEM observations.

Most of the Raman spectra reported so far for the carbon nitride films only consist of two broad bands in the vicinity of 1375 and 1580 cm^{-1} (the so-called D and G bands, respectively) [5,32–36]. The fact that these Raman spectra resemble those of diamond-like or graphitic carbon

films is not too surprising since these films are either amorphous carbon nitrides or heavily nitrogen-doped amorphous carbon films. Recently, Bousetta et al. suggested that the main Raman peak they observed at 1275 cm^{-1} could be attributed to the sp^3 bonding of the carbon nitride [19]. On the other hand, Raman peak at 2140 cm^{-1} is believed to be characteristic of a triple nitrogen–carbon stretch [37] and has been reported by several authors. The present result is, however, the first one in which sharp Raman peaks have been observed for a carbon nitride solid.

Theoretical calculations of the Raman spectra of β-C_3N_4 or α-C_3N_4 or even other C_xN_y structures are not yet available. However, the C–N vibrational frequencies can be estimated from the known Si–N vibrational frequencies by a scaling factor, which in turn can be estimated from the ratios of the bond length and bulk modulus between the two phases, using a Hooke's law approximation [31,32]. With the bond length and bulk modulus suggested by Liu and Cohen [3], we arrive at a scaling factor of 1.44. The calculated Raman vibrational frequencies for both α- and β-C_3N_4, listed in Table 4, are thus obtained by multiplying the Raman shifts for α- and β-Si_3N_4 reported by Wada et al. [31] by 1.44, the scaling factor. For comparison, the observed Raman shifts for our sample are also given in Table 4.

There are a few caveats that need to be noted before we draw any conclusions from the Raman spectra. First, it is well known that the Raman shift is very sensitive to the residual stress in the sample, as well as short-range atomic order and bonding. Most thin film processes, including the MW-PECVD technique used here, are known to introduce significant residual stress in the deposited films. Any departure of the local atomic arrangement from the ideal case also leads to significant variations in the Raman peaks. Second, our film may contain a solid solution of an as-yet unknown $(C; Si)_xN_y$ structure with a wide range of compositions. In this case, there is no calculated Raman spectra with which the observed ones can be compared. Even if we assume the α-$[C(Si)]_3N_4$ structure, one would also expect to see a shift of the observed peak from the calculated position because of the presence of Si. Consequently, for Raman spectra exhibiting many sharp lines in close proximity, such as the ones we observed, erroneous assignment of the line positions might occur due to the possible deviations in the peak positions from the calculated positions.

The last, but not least, point to be made is that the Hooke's law approximation depends strongly on the bulk modulus and the bond length. So far, all the proposed C–N bond lengths are quite similar. However, there is no unique value of the bulk modulus that can be used for the C_3N_4 phase. For instance, Liu and Cohen estimated a bulk modulus comparable to that of diamond [3], whereas Guo and Goddard suggested a value merely half of it [14]. As a result, the scaling factors are 1.44 and 0.91, respectively, using the values suggested by these two groups. Thus, unambiguous identification of the Raman lines can only be made along with more complete structure determinations by other means.

Table 4
Comparison of the measured Raman shifts (cm^{-1}) from Fig. 9 and the calculated β- and α-C_3N_4 Raman shifts. The calculations were based on the Raman shifts of α- and β-Si_3N_4 and scaling the force constants using the results of Liu and Cohen [3]

Measured Raman shift	Calculated Raman shift		Measured Raman shift	Calculated Raman shift	
	β-C_3N_4	α-C_3N_4		β-C_3N_4	α-C_3N_4
199	207		674		677
230		220(s)	688		
259(s)	268(s)		742		740
280		291			773
303(s)*	302(s)		815		819(s)
345	330(s)	333	863(s)		865
355			900	891	
364(s)		372(s)	912		
401		406	938(s)*		
429		429	948(s)		960
439		441	973(s)		995
459		462	1030(s)	1054	1098
487		485			1221
		513(s)		1246	1250
519(s)*		520(s)	1339	1336	1316
		552		1352	1369
566		563			1404
589				1508	1486
619*				1602	1594
664(s)*	649	662			1644

3.5. Role of Si in crystal growth

The incorporation of significant fractions of Si in the crystals was very intriguing in the beginning since no Si-containing gases were used. However, owing to the substrate temperatures as high as 1000–1200 °C, three routes for the incorporation of Si in the crystals during growth are possible: (i) solid state interdiffusion of Si during growth; (ii) evaporation and redeposition of Si, and (iii) the involvement of Si in chemical reactions leading to crystal growth. Based on several observations on the growth of this material reported elsewhere [38], the first two possibilities can be ruled out, and Si has indeed been observed to play a very important catalytic role in promoting the growth of crystalline material. Chemical reactions between the Si substrate and the gaseous species from the plasma are identified as the dominant route for Si incorporation. Notably, similar crystalline material can not be deposited onto non-Si substrates in the absence of Si under otherwise identical deposition conditions, whereas similar crystals can be deposited onto non-Si substrates when placed together with Si substrates in the deposition chamber [38]. More detailed studies are now being carried out to identify the exact role of Si in the growth of these crystals. In addition to the catalytic role of large Si atoms, their incorporation in the crystalline carbon nitride network is also expected to stabilize the resulting network, which may otherwise be highly metastable, since both SiN and GeN are known to be stable crystals, while metastable crystalline CN has not yet been realized despite intense efforts.

4. Conclusions

Si-containing crystalline carbon nitride thin films have been synthesized on Si substrates using microwave plasma-enhanced chemical vapor deposition with a source gas mixture containing CH_4, NH_3 and H_2. Both X-ray photoelectron spectroscopy and Auger electron spectroscopy studies show that Si, C and N are present in the film and that the nitrogen content in the film could reach as high as 50%. Analyses of the XPS peaks indicate that both silicon–nitrogen and carbon–nitrogen bonds are present, whereas silicon–carbon and carbon–carbon bonds are either negligible or not present at all. The absence of the Si–C bond suggests that if Si, C and N are all present in the same crystal, the C and Si must be bridged by nitrogen.

Based on the XRD and TED results, we propose that the structure of these silicon-containing carbon nitride films is close to that of the α-type, with some carbon sites being substituted by silicon atoms. However, nitrogen deficiencies and various levels of Si substitution can cause significant deviations from the ideal α-C_3N_4 structure.

The Raman spectra of these Si-containing carbon nitride films also show many sharp lines, characteristic of crystals with complex structures. However, unambiguous assignment of the line positions is not possible at the present time. We suggest that the Raman spectra of the α-C_3N_4 structure and a similar one with Si and C interchangeably occupying the C sites should be calculated.

The incorporation of Si, together with high substrate temperatures, have been observed to promote the formation of large crystals. It appears that Si plays an important role in enhancing the growth of the crystalline carbon nitride network. Chemical reactions between Si substrate and gaseous species in the plasma have been observed to be a dominant route for Si incorporation. However, the detailed mechanism whereby Si is involved in crystal growth is not clearly understood at present. The incorporation of Si, however, appears to stabilize the hexagonal ternary compound represented by the formula $(C; Si)_xN_y$ with a wide composition range.

Acknowledgements

The authors would like to thank Dr J.C. Lin, Dr Y.L. Wang, Dr H.C. Chang, Professors Y.H. Lee and L.G. Hua for helpful discussions. Technical assistance from Dr M.C. Shih and Mr C.C. Juan is appreciated. M.C. Lin acknowledges the award of a distinguished visiting professorship at IAMS by the National Science Council (NSC) in Taiwan. D.M. Bhusari acknowledges the postdoctoral fellowship awarded also by the NSC in Taiwan. The project is supported by the fund from the NSC, Taiwan, under contract Nos. NSC-85-2113-M-002-025, NSC-85-2113-M-002-027, and NSC-86-2113-M-002-036.

References

[1] In 1984 an unpublished patent disclosure letter was written by C.M. Sung, then at Norton Corporation's Diamond Technology Center. The history was revealed in Diamond Depositions: Science and Technology 5(3), March 1995.
[2] M.L. Cohen, Phys. Rev. B 32 (1985) 7988.
[3] A.Y. Liu, M.L. Cohen, Science 245 (1989) 841; Phys. Rev. B 42 (1990) 10727.
[4] D.J. Jones, A.D. Steward, Phil. Mag. B 46 (1982) 423.
[5] J.H. Kaufman, S. Metin, D.D. Saperstein, Phys. Rev. B 39 (1989) 13053.
[6] C.J. Torng, J.M. Siversten, J.H. Judy, C. Chang, J. Mater. Res. 5 (1990) 2490.
[7] M.Y. Chen, X. Lin, V.P. Dravid, Y.W. Chung, M.S. Wong, W.D. Sproul, Surf. Coat. Technol. 54/55 (1992) 360.
[8] J.F.D. Chubaci, T. Sakai, T. Yamamoto, K. Ogata, A. Abe, F. Fujimoto, Nucl. Instrum. Meth. B 80/81 (1993) 463.
[9] D. Li, Y.W. Chung, M.S. Wong, W.D. Sproul, J. Appl. Phys. 74 (1993) 219.
[10] C. Niu, Y.Z. Lu, C.M. Lieber, Science 261 (1993) 334.
[11] K.M. Yu, M.L. Cohen, E.E. Haller, W.L. Hansen, A.Y. Liu, I.C. Wu, Phys. Rev. B 49 (1994) 5034.
[12] J.P. Riviere, D. Texier, J. Delafond, M. Jaouen, E.L. Mathe, J. Chaumont, Mater. Lett. 22 (1995) 115.
[13] A.Y. Liu, R.M. Wentzcovitch, Phys. Rev. B 50 (1994) 10362.
[14] Y. Guo, W.A. Goddard III, Chem. Phys. Lett. 237 (1995) 72.

[15] Z.J. Zhang, S. Fan, C.M. Lieber, Appl. Phys. Lett. 68 (1996) 2639.
[16] J.J. Cuomo, P.A. Leary, D. Yu, W. Reuter, M. Frisch, J. Vac. Sci. Technol. 16 (1979) 299.
[17] B.R. Stoner, G.-H.M. Ma, S.D. Wolter, J.T. Glass, Phys. Rev. B 45 (1992) 11067.
[18] S. Kumar, T.L. Tansley, Solid State Commun. 88 (1993) 803.
[19] A. Bousetta, M. Lu, A. Bensaoula, A. Schultz, Appl. Phys. Lett. 65 (1994) 696.
[20] H.W. Song, F.Z. Cui, X.M. He, W.Z. Li, H.D. Li, J. Phys.: Condens. Matter 6 (1994) 6125.
[21] F. Fujimoto, K. Ogata, Jpn. J. Appl. Phys. 32 (1993) L420.
[22] D. Marton, K.J. Boyd, A.H. Al-Bayati, S.S. Todorov, J.W. Rabalais, Phys. Rev. Lett. 73 (1994) 118.
[23] A. Hoffman, R. Brener, I. Gouzman, C. Cytermann, H. Geller, L. Levin, M. Kenny, Diamond & Rel. Mater. 4 (1995) 292.
[24] L. Kubler, J.L. Bischoff, D. Bolmont, Phys. Rev. B 38 (1988) 13113.
[25] J.H. Scofield, J. Electron. Spectrosc. Relat. Phenomena 8 (1976) 129.
[26] W. Kern, R.S. Rosler, J. Vac. Sci. Technol. 14(5) (1977) 1082.
[27] D.M. Bhusari, C.K. Chen, K.H. Chen, T.J. Chuang, L.C. Chen, M.C. Lin, J. Mater. Res. 12 (1997) 322.
[28] X-ray diffraction data of SiN are listed in powder files nos. 9-250 and 9-259.
[29] E.E. Haller, M.L. Cohen, W.L. Hansen, US Patent No. 5110679 (1992).
[30] L.C. Chen, C.Y. Yang, D.M. Bhusari, K.H. Chen, M.C. Lin, J.C. Lin, T.J. Chuang, Diamond & Rel. Mater. 5 (1996) 514.
[31] N. Wada, S.A. Solin, I. Wong, S. Prochazka, J. Non-Cryst. Solids 43 (1981) 7.
[32] M.R. Wixom, J. Am. Ceram. Soc. 73(7) (1990) 1973.
[33] L. Maya, D.R. Cole, E.W. Hagaman, J. Am. Ceram. Soc. 74 (1991) 1686.
[34] M.Y. Chen, D. Li, X. Lin, V.P. Dravid, Y.W. Chung, M.S. Wong, S. Sproul, J. Vac. Sci. Technol. A 11 (1993) 521.
[35] G. Mariotto, F.L. Freire, Jr., C.A. Achete, Thin Solid Films 241 (1994) 255.
[36] F. Rossi, B. Andre, A. Veen, P.E. Mijnarends, H. Schut, F. Labohm, H. Dunlop, M.P. Delplancke, F. Hubbard, J. Mater. Res. 9 (1994) 2440.
[37] Z.M. Ren, Y.C. Du, Y. Qiu, J.D. Wu, Z.F. Ying, X.X. Xiong, F.M. Li, Phys. Rev. B 51 (1995) 5274.
[38] D.M. Bhusari, C.K. Chen, K.H. Chen, L.C. Chen, T.J. Chuang, Mater. Res. Soc. Proc. 441 (1997), in press.